PAPER

Mechanisms of microexplosion-accelerated pyrolysis and oxidation of lithium-containing droplets: an atomistic perspective†

Ruitian He[a] and Kai H. Luo ⓘ *[a,b]

Microexplosion has been extensively studied in the context of fuel spray and droplet evaporation in engines, while its existence, impact and atomistic insight have rarely been explored in the context of flame synthesis of nanoparticles. In this study, reactive force-field molecular dynamics simulations are performed to elucidate the mechanisms of pyrolysis and oxidation of an isolated lithium nitrate nanodroplet. During the pyrolysis process, the nucleation and growth of a bubble are observed inside the droplet, which should be ascribed to the release of nitrogen and oxygen gases from the decomposition of lithium nitrate, ultimately leading to rapid droplet fragmentation (microexplosion). To demonstrate the role of microexplosion with various intensities, *via* altering ambient temperature and addition of oxygen gas into the environment, thorough analyses of bond reactions, droplet morphology and compounds of the synthesized lithium nanoparticles are carried out. With elevated ambient temperature, the droplet substantially expands due to bubble growth and the time required for droplet disruption is shortened, which implies the enhanced strength of microexplosion. Simultaneously, the connection between the lithium and other atoms becomes weak, as evidenced by a decrease in the number of lithium bonds. These give rise to a reduction in the quantity of large-sized lithium agglomerates and simultaneously an increase in the amount of fine lithium nanoparticles. To further clarify the reaction mechanism for a lithium-containing droplet under various ambient conditions, three reaction modes, *i.e.*, core–shell diffusion-controlled, microexplosion-accelerated and microexplosion-dominated, are distinguished based on the intensity of microexplosion and the quality of synthesized lithium nanoparticles. Fine lithium-containing nanoparticles are expected to be produced in the microexplosion-dominated mode under high temperature conditions.

Introduction

Flame spray synthesis (FSP), involving the atomization and evaporation of precursor solution, followed by pyrolysis, oxidation, coagulation and sintering processes,[1,2] has emerged as one of the most reliable and versatile methods to manufacture nanostructured electrode materials for next-generation lithium-ion batteries (LIBs).[3–5] A thorough understanding of physicochemical mechanisms in pyrolysis and oxidation is a prerequisite for the production of well-structured homogeneous nanomaterials. Notably, two reaction paths for nanoparticle synthesis *via* FSP have gained widespread acceptance

in the academic community and are the droplet-to-particle and gas-to-particle routes, respectively.[6] Generally, the former is associated with the precursor solution with low combustion enthalpy density and consequently leads to the formation of inhomogeneous particles owing to incomplete droplet evaporation. In contrast, the latter is the dominant path for producing homogeneous ultrafine nanoparticles, where the decomposition temperature of the precursor is lower than the boiling point of the solvent component and the combustion enthalpy density is sufficient.[6]

Taking into account the volatility differences in practical precursors, superheating of the highly volatile component is likely to occur in the droplet interior owing to the finite mass diffusion rate in the liquid phase.[5] Besides, the precursor is highly likely to decompose into gaseous products at exceedingly high combustion temperatures and then will be trapped in the droplet interior.[1] These will give rise to a pressure difference inside and outside the droplet, ultimately leading to the occurrence of microexplosion characterized by a rapid droplet

[a]Department of Mechanical Engineering, University College London, Torrington Place, London WC1E 7JE, UK. E-mail: k.luo@ucl.ac.uk
[b]Shanghai Institute for Advanced Study, Zhejiang University, Shanghai 201203, China
†Electronic supplementary information (ESI) available. See DOI: https://doi.org/10.1039/d4nr00592a

disruption, which has received increasing interest in nano-material synthesis.[1,3,4] Microexplosion is usually associated with improved atomization of precursor droplets and the desired products of fine-sized homogeneous nanoparticles *via* FSP.[3,4] However, most existing research studies[7–9] focus on the impact of microexplosion on the evaporation and combustion characteristics of fuel spray and droplets within the context of diesel engines.

Several experimental investigations[10–12] have been carried out to understand the role of microexplosion in the chemical reactions of metal precursors in nanoparticle synthesis. Rosebrock *et al.*[10] for the first time demonstrated the occurrence of microexplosion in a single burning droplet comprising metal oxides. They emphasized the prominent role of microexplosion in the synthesis of homogeneous nanoparticles, along with the minimal impact of precursor evaporation and solvent composition. Nevertheless, microexplosion can exert a negative effect on the synthesis of fine nanoparticles. Hollow inhomogeneous agglomerates can be obtained even with microexplosion, which can be clarified by the accumulation of condensed vapor at the droplet surface and the ultimate flame extinction. Considerable research studies have been directed towards elucidating the mechanism underlying microexplosion in nanomaterial synthesis.[11–13] Tang *et al.*[12] visualized the dynamics of burning micron-sized aluminum agglomerations using a flat-flame burner at ambient temperatures ranging from 800 to 1800 K and ambient oxygen concentrations spanning from 0.5 to 5.5 mol m^{-3}. Considering that the measured droplet temperature at the onset of microexplosion is close to the boiling point of aluminum, microexplosion is speculated to occur resulting from the evaporation of aluminum in the droplet interior. Li *et al.*[13] employed rainbow spectroscopy to measure the evolution of droplet size as well as the liquid core and surface temperatures for a burning droplet with microexplosion. Their results indicate the formation of a core–shell structure in the droplet, as evidenced by a sudden temperature enhancement at the droplet core and surface as well as a dramatic decrease in the mass fraction of xylene at the droplet surface. The highly volatile component is expected to be superheated and then the produced vapor is trapped inside the droplet, which eventually results in the onset of microexplosion.

Numerous numerical studies have been conducted to understand the mechanism of microexplosion, and many criteria have been proposed to identify the occurrence of microexplosion.[14–16] Law[14] developed one of the first microexplosion models for multi-component miscible droplets based on the experimental and fitted limits of superheat. In his model, spontaneous evaporation occurs within the droplet when the limit of superheat is locally reached, which would lead to the generation of internal bubbles and consequently microexplosion (or droplet fragmentation). Zeng and Lee[15] proposed a microexplosion model by describing bubble generation using homogeneous nucleation theory.[16] Droplet fragmentation is hypothesized to occur when a disturbance variable, depending on the droplet and internal bubble sizes,

exceeds a constant threshold. Despite the fact that great efforts have been made in the numerical modelling of microexplosion, few studies have been devoted to gaining an atomistic insight into the chemical reactions associated with microexplosion during nanomaterial synthesis,[17] to the best of our knowledge. Some researchers[18–21] employed the classical molecular dynamics (MD) simulation method to understand the physics of microexplosion. However, the classical MD method is only applicable for nonreactive interactions, inaccessible when simulating chemical reactions due to its limited description of atom connectivity. This gives rise to the development of a method recognized as the reactive force-field (ReaxFF).[22–24] The ReaxFF is capable of gaining fundamental insight into chemical reactions, because it enables the predictions of bond breaking and formation through an empirical bond-order formalism optimized based on a training set of quantum mechanics (QM) calculations and experimental data.[23] Li *et al.*[17,25] conducted ReaxFF simulations to simulate the micro-explosion-facilitated oxidation of molten aluminum nanoparticles. Their simulation results show that the violent evaporation of aluminum inside the nanodroplet leads to the formation of hot spots inside the droplet and the occurrence of microexplosion. Three oxidation routes for aluminum nanoparticles are identified under a wide range of ambient conditions, suggesting a promising possibility for unravelling the atomistic details of chemical reactions in the synthesis of LIB nanomaterials.

Several investigations into the key parameters governing the production of nanoparticles, *e.g.*, the ambient oxygen concentration,[7,17] ambient temperature[17,26] and precursor composition,[26,27] have been conducted. Tang *et al.*[12] identified that the microexplosion of an aluminum droplet only occurs when the ambient oxygen concentration exceeds a threshold value. This is because the agglomerate temperature reaches the boiling point of volatile aluminum with an enhanced heat conduction rate in an oxygen-abundant ambient environment, consequently leading to the synthesis of fine nanoparticles assisted by microexplosion. Additionally, the surrounding temperature is believed to have a substantial influence on the phase change, bubble growth rate and microexplosion characteristics of the droplet, ultimately altering the quality of metal oxide nanoparticles.[7,28]

Though extensive efforts have been made to understand the mechanisms of reactions with microexplosion in FSP, direct experimental measurements for burning droplets and sprays with microexplosion are still lacking.[1,3] The underlying physics of bubble nucleation (or microexplosion) has not been fully understood. Whether microexplosion stems from the preferential evaporation of the low-volatile component or the release of gases produced from the thermal decomposition remains unresolved. Besides, many crucial issues, *e.g.*, the exact occurrence of bubble nucleation, degree of superheating and vapor composition, are hardly accessible by experimental investigations due to the small size of droplets in sprays and the limited resolution of existing high-speed cameras.[17] Moreover, previous studies have focused almost exclusively on the

measurement of morphological changes of synthesized nano-particles or agglomerates. However, the intrinsic mechanism of chemical reactions during pyrolysis or oxidation remains obscure.

The aim of this study is to fill this gap by providing an atomistic insight into the mechanism of nanoparticle synthesis accompanied by microexplosion using reactive molecular dynamic simulations. The precursor is lithium nitrate (LNT) dissolved in water, which is one of the common choices for the precursors in nanomaterial synthesis for LIBs. The impact of ambient temperature and the presence of oxygen in the ambient environment on the droplet microexplosion, bond connection and quality of synthesized nanoparticles will be comprehensively explored. The reaction modes will be categorized to provide a better understanding of the relationship between the microexplosion intensity and metal nanoparticle synthesis with respect to different ambient conditions.

Simulation methodology and setup

In this study, ReaxFF molecular dynamics simulations[23] implemented in the LAMMPS package[29] are conducted. The Li/N/O/H ReaxFF force field optimized by Yang *et al.*[30] based on QM calculations is adopted. This interatomic potential has been extensively validated against the experimental and QM calculation results, including the bond dissociation energy in water molecules, the equation of state of Li with a bcc structure and Li_2O crystalline phases. A bond-order cutoff of 0.3 Å is adopted in this study to determine the bond connection among various atoms, which is a commonly used criterion in ReaxFF MD simulations.[24,31]

A spherical precursor droplet with an initial diameter of 10 nm is constructed in a cubic simulation box with an edge length of 40 nm. The precursor is composed of lithium nitrate dissolved in water with a solution concentration of 5.4 mol L^{-1} H_2O.[26] The ambient pressure is set as 0 (vacuum) and 1 MPa to simulate the pyrolysis and oxidation processes of the LNT droplet, respectively, and the ambient temperature varies from 1500 to 3000 K. The vacuum environment is an ideal setup for pyrolysis studies, which avoids any oxidative reactions. The simulation case under 1 MPa pressure closely resembles the realistic conditions of flame spray pyrolysis,[3,26] in which the high-temperature ambient environment is occupied by oxygen molecules. Detailed information about the initial configuration is provided in our previous works.[26,31] Prior to each simulation, the minimization of potential energy is performed with the conjugated gradient (CG) algorithm. Then, ReaxFF MD simulations are carried out by employing a canonical ensemble (*NVT*) with a constant number of particles (*N*), volume (*V*) and temperature (*T*). Periodic boundary conditions in three dimensions and a timestep of 0.1 fs are applied. In addition, the Nosé–Hoover thermostat[32] is utilized to raise the droplet temperature during the heating-up period and maintain a constant temperature for the whole simulation system with a damping parameter of 10 fs. The thickness of the stat-istical bin is set to be 0.1 nm based on our sensitivity analysis for the number of atoms in each bin.

Results and discussion

Pyrolysis of an Li-containing droplet with microexplosion

In this section, the mechanism of pyrolysis of an isolated LNT nanodroplet with microexplosion is investigated in a vacuum environment. During the initial heating-up period, the droplet is heated up to 2000 K (T_a = 2000 K) within the first 10 ps using the Nosé–Hoover thermostat,[32] and then an *NVT* ensemble is employed for the whole simulation system. In this study, the occurrence of microexplosion is defined as the time when the droplet bursts,[15,19] indicated by the peak in the variation rate of the droplet diameter, and the lifetime of the droplet is defined from the start to the occurrence of microexplosion. The interface between the liquid phase and ambient environment is determined using the widely used '90-10' approach,[33,34] where the outer and inner interfacial densities are calculated as $0.1\rho_l + 0.9\rho_v$ and $0.9\rho_l + 0.1\rho_v$, respectively. ρ_l and ρ_v refer to the densities of the liquid phase and ambient environment, respectively. Fig. 1(a) depicts the radial distribution of density and snapshots of the droplet at different
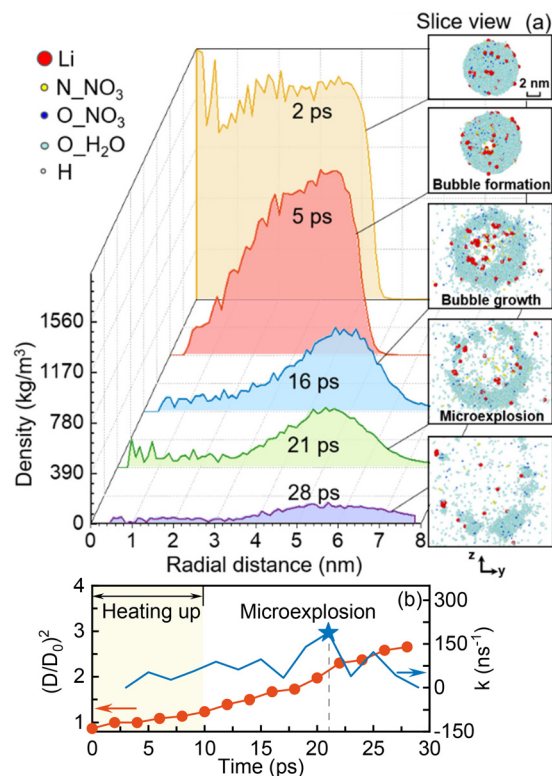

Fig. 1 Dynamics of the pyrolysis of an isolated LNT droplet with microexplosion. (a) Radial distribution of density and snapshots of the droplet at different time points. (b) Temporal evolution of the normalized droplet diameter squared and its variation rate, T_a = 2000 K. The origin is defined as the mass center of the droplet and the star symbol signifies the occurrence of microexplosion for the droplet.

time points and Fig. 1(b) presents the temporal evolution of the normalized droplet diameter squared and its variation rate. During the initial heating-up period (before 10 ps), the droplet diameter squared keeps rising, which seems to be inconsistent with the observed trend of a decrease followed by a rapid increase in droplet size over time in most existing experiments.[11,27] This is due to the more pronounced bubble growth inside the droplet and thermal swelling with elevating temperature. A similar trend to that captured in the experiments will be discussed at a lower ambient temperature in the next section. Meanwhile, the density at the droplet core is diminished to zero at 5 ps with a hollow structure in the slice view in Fig. 1(a). These phenomena suggest the potential occurrence of bubble nucleation inside the droplet. Nevertheless, the inherent physics behind this phenomenon remains unclear. Whether it originates from gaseous production during the pyrolysis or preferential evaporation of the highly volatile component in the precursor solution is still controversial.

To verify the occurrence of bubble nucleation and unravel its intrinsic physics, the temporal evolution of the normalized numbers of lithium compounds, gaseous products and bond numbers is illustrated in Fig. 2(a), (b) and (c), respectively. Additionally, the density profiles of nitrogen atoms at different time points are presented in Fig. 2(d). During the early heating-up period, the amount of NO_x resulting from the pyrolysis of nitrates, e.g., NO_2 and NO,[35] is dramatically reduced over time. This can be ascribed to the decomposition of NO_x into oxygen and nitrogen gases, as shown in Fig. 2(b), evidenced by the breakup of N–O bonds in NO_x and the subsequent formation of N–N bonds, as shown in Fig. 2(c). As the oxygen and nitrogen gases are the primary products resulting from the decomposition of nitrate[36] at temperature exceeding the decomposition temperature of LNT (>913 K),[3] the decomposition of LNT is highly likely to occur during the initial heating-up period. Besides, the nitrogen atom progressively accumulates at the droplet core over time, as illustrated in Fig. 2(d), which suggests the gradual liberation of nitrogen gas. Therefore, it can be inferred that the bubble nucleation should be attributed to the release of gases produced from the thermal decomposition of the LNT precursor.

Over time, the internal bubble rapidly expands, as inferred from the enlargement of the low-density region within the droplet core and the hollow structure illustrated in Fig. 1(a). This leads to a substantial increase in the droplet diameter, as depicted in Fig. 1(b). Notably, microexplosion of the droplet is observed to take place at 21 ps with an opening circular shape of the droplet, as shown in Fig. 1(a). The variation rate of the normalized droplet diameter squared (k) peaks at 180 ns^{-1}, which also hints at the burst of the bubble inside the droplet. Simultaneously, from 10 ps onward, the normalized number of lithium oxides (Li_xO_y), which are the desirable products in FSP, demonstrates a slight increase with a progressively rising variation rate. In contrast, the amount of large-sized lithium complexes $Li_nN_xH_yO_z$ significantly reduces. This can be interpreted by the almost constant Li–O bond number as well as
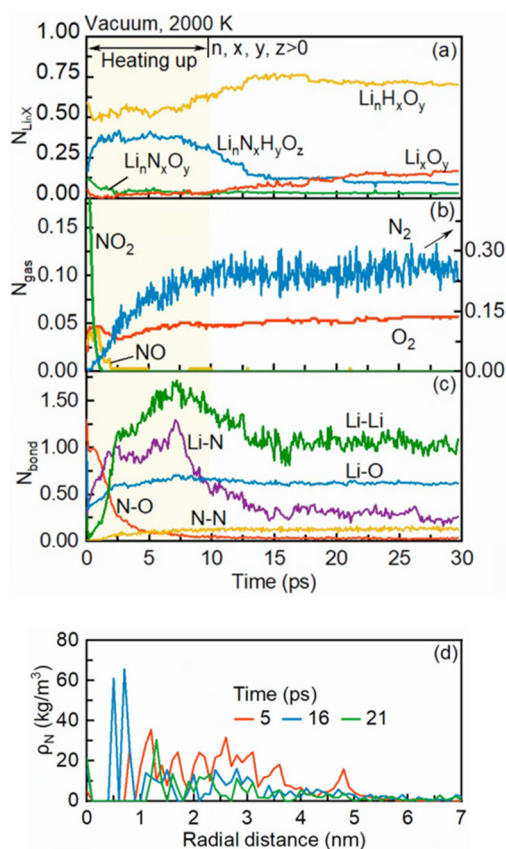

Fig. 2 Temporal evolution of the normalized numbers of (a) lithium compounds and (b) gaseous products during the pyrolysis of an isolated LNT droplet. (c) Number of bonds (d) radial distribution of nitrogen atoms at various time points, T_a = 2000 K. The normalized number of Li_nX is calculated as $n \cdot m/N_{LNT}$, where m is the number of molecules or bonds and N_{LNT} is the initial molecular number of lithium nitrate. For gases excluding N_2, the normalized number is determined by dividing their number of molecules by N_{LNT} (i.e., m/N_{LNT}), whereas for N_2 it is calculated as $2m/N_{LNT}$.

the reducing numbers of Li–Li and Li–N bonds, as described in Fig. 2(c). A detailed illustration of the microexplosion role in these synthesized products will be explored as follows.

Effect of ambient temperature on the pyrolysis of an Li-containing droplet with microexplosion

In this section, a series of comparative studies with the ambient temperature spanning from 1500 to 3000 K are performed. The simulation settings of the heating-up period and vacuum environment remain the same as those in the Pyrolysis of an Li-containing droplet with microexplosion section, in which the droplet is heated up to a desired value in 10 ps using the Nosé–Hoover thermostat.[32] To evaluate the intensity of microexplosion, the temporal evolution of the droplet diameter squared is displayed in Fig. 3. The dashed lines and numbers near the curves represent the slope of curves at the end of the droplet lifetime and their variation rate. With the ambient temperature elevated from 2000 to 3000 K, the normalized droplet diameter squared undergoes a
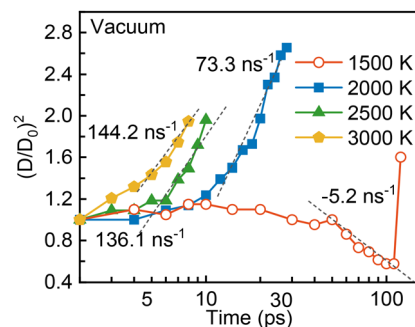
Fig. 3 Temporal evolution of the normalized diameter squared of an isolated LNT droplet accompanied by microexplosion at T_a = 1500−3000 K. $(D/D_0)^2$ refers to the normalized droplet diameter squared, and the dashed lines and numbers near the curves refer to the slope of curves and their variation rate with units of ns^{-1}, respectively. The variation rate plateaus at the end of curves, implying droplet fragmentation.

Fig. 4 Temperature effect on the formation of lithium compounds: (a) normalized number of Li–Li bonds, (b) normalized number of Li–N bonds, (c) normalized number of Li–O bonds, and (d) proportion of lithium compounds when the droplet disrupts at T_a = 1500−3000 K. The normalized time in (a), (b) and (c) is determined by dividing the time by the occurrence of microexplosion.

similar rapid increase to that at 2000 K but with a steeper slope. Additionally, the variation rate of the droplet diameter squared enhances from 73.3 to 144.2 ns^{-1}. Moreover, the elevating ambient temperature causes droplet disruption and thus the droplet lifetime undergoes a substantial reduction. These suggest that the rising ambient temperature speeds up the microexplosion and elevates the strength of microexplosion.

To evaluate the influence of microexplosion with various intensities on the bond reactions and products of nanoparticles, the temporal evolution of the normalized numbers of Li–Li, Li–N and Li–O bonds and the proportions of lithium compounds after the occurrence of microexplosion at different ambient temperatures are shown in Fig. 4(a), (b), (c) and (d), respectively. With increasing ambient temperature, the normalized numbers of lithium bonds sharply decrease, as shown in Fig. 4(a), (b) and (c). Taking the Li–Li bond as an example, as the ambient temperature increases from 2000 to 3000 K, the peak value of the normalized number of Li–Li bonds is diminished from 1.8 to 1.5, as shown in Fig. 4(a), which leads to a lower probability of forming lithium clusters. As depicted in Fig. 4(d), the proportion of $Li_mH_xO_y$ ($m > 2$) shows a general diminished trend, reducing from 22 to 12% as the ambient temperature rises from 2000 to 3000 K, while that of $Li_nH_xO_y$ ($n \leq 2$) containing fewer lithium atoms steadily increases. This phenomenon suggests microexplosion with greater intensity as the elevated ambient temperature suppresses the agglomeration of metal atoms. Notably, unlike Li–N and Li–O bonds, the normalized number of Li–Li bonds is always greater than unity, as indicated by the grey line in Fig. 4(a). This can be justified by the small size of the lithium atom and the high coordination number ranging from 2 to 8 measured in the experiments.[37]

In contrast to the high ambient temperature conditions spanning from 2000 to 3000 K, the LNT droplet manifests completely different behaviors at a relatively low ambient temperature (1500 K), which is nevertheless consistent with 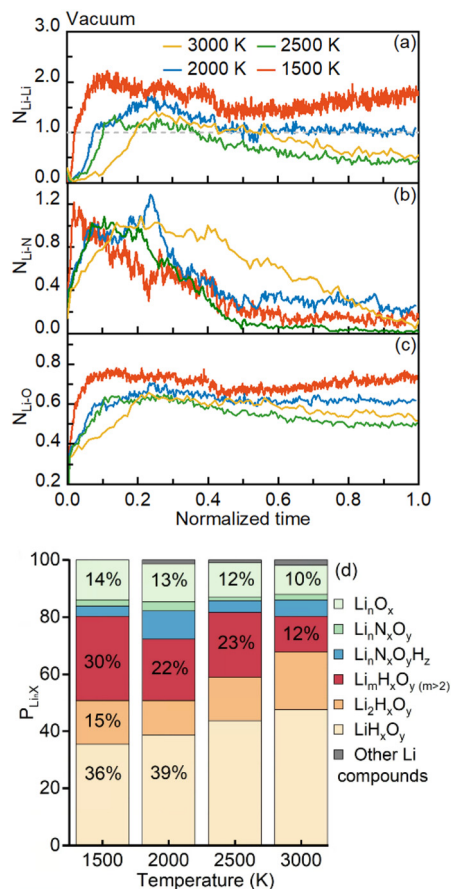the results in most existing experiments on millimeter- or micrometer-sized droplets.[11,27] A non-linear tendency of the normalized droplet diameter squared over time is shown in Fig. 3. A slightly swollen droplet and a nearly constant droplet diameter are captured before 40 ps. This can be interpreted by the competition between the internal bubble growth and precursor depletion due to evaporation and reaction, which is in accord with the experimental result of a millimeter droplet exposed to a furnace with a relatively low ambient temperature ranging from 773 to 1073 K.[27] After 50 ps, the droplet gradually shrinks due to high evaporation and reaction rates, implying the absence of violent microexplosion and the abrupt change of droplet size. Correspondingly, during the pyrolysis without strong microexplosion, more agglomerated lithium clusters are expected to form at the end of the droplet lifetime. As depicted in Fig. 4(d), as the ambient temperature decreases from 2000 to 1500 K, the proportion of $Li_mH_xO_y$ ($m > 2$) rapidly enhances from 22 to 30%, whereas the amount of LiH_xO_y is reduced from 39 to 36%. This phenomenon also confirms the positive effect of microexplosion on the synthesis of Li-containing fine nanoparticles at elevated ambient temperature.

Reaction mechanisms of an Li-containing droplet with microexplosion

In this section, the reaction mechanisms of an isolated LNT nanodroplet in the presence of ambient oxygen are elucidated. The ambient temperature is set at relatively low values, specifically 1500 and 2000 K, to achieve a comprehensive understanding of the mechanism of reactions with low reaction rates. The ambient pressure is maintained at 1 MPa in the presence of oxygen in the surroundings, surpassing the pressure in the realistic FSP process. This technique is commonly employed to accelerate MD simulations.[26,38] Fig. 5 and 6 present a series of snapshots of the dynamics of an LNT droplet as well as the normalized number of Li_nX ($n > 0$) after the droplet fragmentation and temporal evolution of lithium oxides under the conditions in the presence and in the absence of oxygen at 1500 K.

The presence of oxygen in the ambient environment is recognized to affect the droplet disruption and the formation of lithium nanoparticles at 1500 K. Primarily, the droplet structure is greatly altered during the reaction. In a vacuum environment, a core–shell structure is captured at 42 ps, as presented in Fig. 5(b), where the lithium atoms agglomerate in the inner region, while other atoms are distributed in the outer layer. Conversely, in the presence of ambient oxygen gas, a more homogeneous distribution of lithium atoms is observed inside the droplet. This is because of the elevated heat transfer rate from the high pressure ambient environment to the droplet after the initial heating-up period (after 10 ps), which leads to accelerated atom motions and ultimately a more homogeneous distribution of lithium atoms and a decreased quantity of lithium agglomerates within the droplet. Besides, the disruption events of the droplet are varied in the presence of ambient oxygen gas. Under the ambient oxygen concentration, prior to the final fragmentation, the formed bubble shifts from the inner region to the droplet surface starting at 58 ps and results in puffing at 70 ps, as displayed in Fig. 5(a). It is worth mentioning that puffing, generally regarded as a weak microexplosion accompanied by the deformation of the droplet, is characterized by gas ejection near the droplet surface.[39,40] Alternatively,
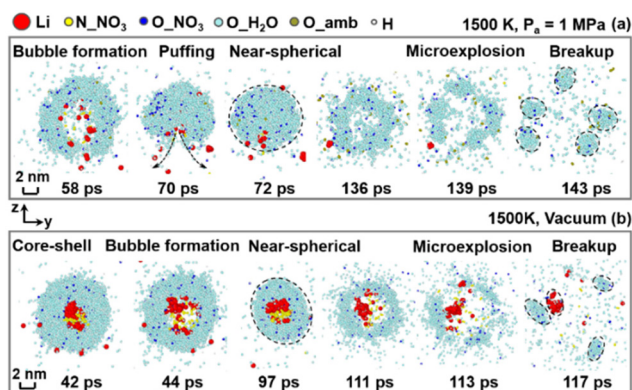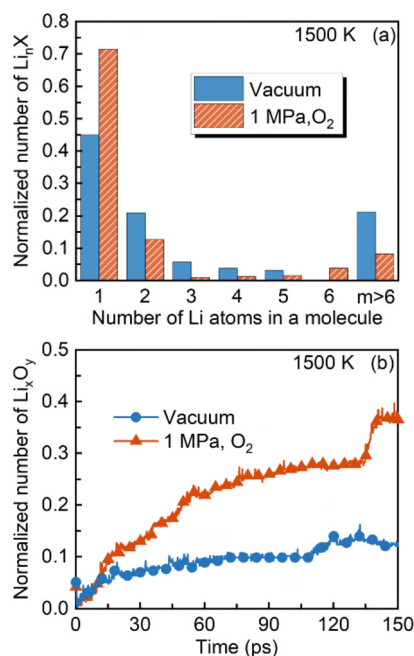

Fig. 6 O$_2$ effect on (a) the probability distribution of the number of lithium atoms in a molecule and (b) the normalized number of lithium oxides generated during the pyrolysis or oxidation of an isolated LNT droplet after the droplet disruption (at 150 ps) at T_a = 1500 K.

in the absence of oxygen, though the bubble is observed to nucleate inside the droplet at 44 ps, the droplet does not undergo a noticeable microexplosion but only deforms into a near-spherical shape at 97 ps, as presented in Fig. 5(b).

Most importantly, the size and compounds of the synthesized Li-containing nanoparticles are changed. In the absence of ambient oxygen, several lithium clusters are observed, persisting even after the droplet fragmentation (at 117 ps), as shown in Fig. 5(b), whereas the lithium agglomerates cannot be captured throughout the entire droplet lifetime under the oxygen conditions, as shown in Fig. 5(a). The large reduction in the amount of Li_nX comprising more than one lithium atom ($n > 1$) and the substantial increase in LiX, as shown in Fig. 6(a), also signify the refined size of the synthesized nanoparticles. This should be attributed to the accelerated heat transfer process from the high-pressure and temperature ambient environment to the droplet interior after the heating-up period and consequently the enhanced intensity of microexplosion, compared to that in the vacuum environment.[6,26] Additionally, the amount of the desired Li_xO_y products substantially increases from 0.12 to 0.36 at 150 ps in the presence of ambient oxygen, as depicted in Fig. 6(b). To better identify the impact of ambient gas, a comparative study using three simulation systems under vacuum, nitrogen gas and oxygen gas conditions has been provided in Fig. S1 and S2 in the ESI.†

To clarify the reaction mechanisms of the Li-containing precursor droplet under a wide range of ambient conditions, three reaction modes of the LNT droplet are identified, i.e., core–shell diffusion-controlled, microexplosion-accelerated and microexplo-

Fig. 5 Snapshots (slice view) of the dynamics of an LNT droplet under (a) O$_2$ conditions and (b) vacuum conditions at T_a = 1500 K.
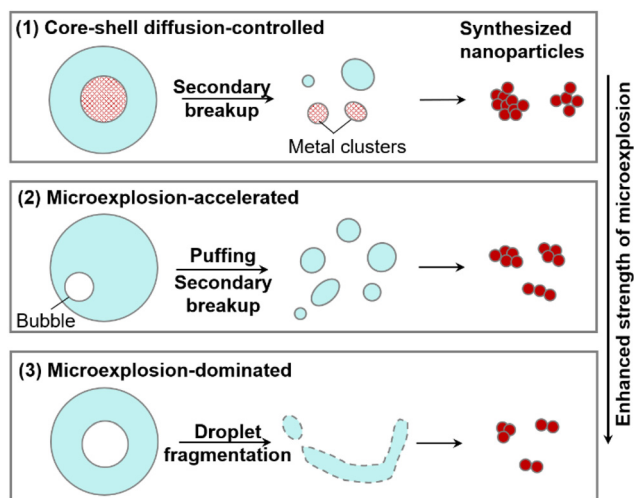
Fig. 7 A schematic of three reaction modes for an isolated lithium-containing droplet accompanied by microexplosion with various intensities.

sion-dominated modes, as presented in Fig. 7. Primarily, in the low-temperature vacuum environment, the pyrolysis of LNT can be identified as the core–shell diffusion-controlled reaction, characterized by a core–shell structure owing to the finite mass diffusion rate inside the droplet. Microexplosion does not occur instantaneously after the bubble nucleation. Instead, the droplet appears to deform into a near-spherical shape and ultimately bursts into multiple child droplets, which would probably lead to the undesired formation of large-sized inhomogeneous lithium agglomerates. Secondly, in the low-temperature environment in the presence of oxygen, the reaction mechanism transitions into the microexplosion-accelerated mode. Prior to the ultimate droplet disruption, puffing, droplet deformation and secondary breakup take place. The intensified microexplosion facilitates the formation of fine Li-containing nanoparticles. Lastly, the microexplosion-dominated mode is demonstrated at very high ambient temperatures. A strong microexplosion takes place promptly after the nucleation and growth of the bubble inside the droplet, which significantly accelerates the synthesis of fine Li-containing nanoparticles and suppresses particle agglomeration due to the weakened bond connection between lithium and other atoms.

Conclusions

Fundamental investigations have been performed to unravel the role of microexplosion in the pyrolysis and oxidation processes of a lithium nitrate nanodroplet as well as the synthesis of lithium nanoparticles by the ReaxFF MD simulation method. The primary conclusions are as follows:

(1) The bubble nucleation inside the lithium nitrate droplet should be attributed to the release of nitrogen and oxygen gases produced from the decomposition of lithium nitrate. As the internal bubble grows, the droplet progressively expands and ultimately microexplosion takes place, characterized by a peak value of the droplet diameter and rapid fragmentation.

(2) The pyrolysis and oxidation of a single lithium nitrate nanodroplet can be categorized into three types, *i.e.*, core–shell diffusion-controlled, microexplosion-accelerated and microexplosion-dominated modes, characterized by a progressively elevating intensity of microexplosion. The synthesis of fine lithium-containing nanoparticles is expected to occur in the microexplosion-dominated mode under high-temperature conditions.

(3) Microexplosion plays an essential role in the synthesis of lithium-containing nanoparticles during the pyrolysis and oxidation processes of a precursor nanodroplet and its impact greatly varies with respect to the surrounding conditions. As the ambient temperature elevates, the microexplosion of the droplet becomes more violent, as inferred by the substantial enhancement in droplet size and reduced time required for droplet disruption. Meanwhile, the bond connection between the lithium and other atoms becomes weak. These give rise to a lower probability of lithium agglomeration and therefore a larger quantity of fine-sized lithium-containing nanoparticles.

Author contributions

Ruitian He: conceptualization, methodology, software, validation, investigation, visualization, and writing – original draft. Kai H. Luo: conceptualization, project administration, funding acquisition, supervision, and writing – review and editing.

Data availability

The data supporting this article have been included as part of the ESI.†

Conflicts of interest

There are no conflicts to declare.

Acknowledgements

References

1 D. S. Jung, Y. N. Ko, Y. C. Kang and S. B. Park, *Adv. Powder Technol.*, 2014, **25**(1), 18–31.
2 J. S. Park, J. K. Kim, J. H. Hong, J. S. Cho, S. K. Park and Y. C. Kang, *Nanoscale*, 2019, **11**, 19012–19057.

3 F. Meierhofer, H. Li, M. Gockeln, R. Kun, T. Grieb, A. Rosenauer, U. Fritsching, J. Kiefer, J. Birkenstock, L. Mädler and S. Pokhrel, *ACS Appl. Mater. Interfaces*, 2017, **9**(43), 37760–37777.

4 M. F. Stodt, C. Liu, S. Li, L. Maedler, U. Fritsching and J. Kiefer, *Proc. Combust. Inst.*, 2021, **38**(1), 1711–1718.

5 M. F. Stodt, J. D. Groeneveld, L. Maedler, J. Kiefer and U. Fritsching, *Combust. Flame*, 2022, **240**, 112043.

6 S. Pokhrel and L. Mädler, *Energy Fuels*, 2020, **34**(11), 3209–13224.

7 M. Mikami and N. Kojima, *Proc. Combust. Inst.*, 2002, **29**(1), 551–559.

8 H. Watanabe and K. Okazaki, *Proc. Combust. Inst.*, 2013, **34**(1), 1651–1658.

9 T. Kadota, H. Tanaka, D. Segawa, S. Nakaya and H. Yamasaki, *Proc. Combust. Inst.*, 2007, **31**(2), 2125–2131.

10 C. D. Rosebrock, N. Riefler, T. Wriedt, L. Mädler and S. D. Tse, *AIChE J.*, 2013, **59**(12), 4553–4566.

11 C. Kong, Y. Wang, Y. Qian, X. Wu and Z. Zhang, *Proc. Combust. Inst.*, 2023, **39**, 3489–3495.

12 Y. Tang, C. Kong, Y. Zong, S. Li, J. Zhuo and Q. Yao, *Proc. Combust. Inst.*, 2017, **36**, 2325–2332.

13 H. Li, C. D. Rosebrock, Y. Wu, T. Wriedt and L. Mädler, *Proc. Combust. Inst.*, 2019, **37**(1), 1203–1211.

14 C. K. Law, *AIChE J.*, 1978, **24**, 626–632.

15 Y. Zeng and C. F. Lee, *Proc. Combust. Inst.*, 2007, **31**(2), 2185–2193.

16 C. T. Avedisian and I. Glassman, *J. Heat Transfer*, 1981, **103**, 272–280.

17 G. Li, L. Niu, W. Hao, Y. Liu and C. Zhang, *Combust. Flame*, 2020, **214**, 238–250.

18 T. P. Senftle, S. Hong, M. M. Islam, S. B. Kylasa, Y. Zheng, Y. K. Shin, C. Junkermeier, R. Engel-Herbert, M. J. Janik, H. M. Aktulga, T. Verstraelen, A. Grama and A. C. T. van Duin, *npj Comput. Mater.*, 2016, **2**(1), 1–14.

19 M. Wei, S. Yang, H. Ju and G. Guo, *Int J. Heat Mass Transfer*, 2022, **196**, 123263.

20 M. Wei, S. Yang, G. Guo, B. Yuan, S. Wu, H. Ju and Z. Wang, *Appl. Therm. Eng.*, 2024, **241**, 122334.

21 G. Nagayama, T. Tsuruta and P. Cheng, *Int. J. Heat Mass Transfer*, 2006, **49**(23), 4437–4443.

22 F. A. Soria and C. D. Valentin, *Nanoscale*, 2021, **13**, 4151–4166.

23 A. C. T. van Duin, S. Dasgupta, F. Lorant and W. A. Goddard, *J. Phys. Chem. A*, 2001, **105**, 9396–9409.

24 Q. Mao, S. Rajabpour, M. K. Talkhoncheh, J. Zhu, M. Kowalik and A. C. T. van Duin, *Nanoscale*, 2022, **14**, 6357–6372.

25 G. Li, L. Niu, Y. Liu and C. Zhang, *Energ. Mater. Front.*, 2021, **2**(1), 40–50.

26 D. Hou, G. Wang, J. Gao and K. H. Luo, *Nanoscale*, 2023, **15**, 5877–5890.

27 I. Javed, S. W. Baek and K. Waheed, *Exp. Therm. Fluid Sci.*, 2014, **56**, 33–44.

28 B. Wu, X. Wang, Y. Zhu, H. Wu, A. He, H. Wu and P. Wang, *J. Phys. Chem. C*, 2023, **127**(34), 16781–16791.

29 S. Plimpton, *J. Comput. Phys.*, 1995, **117**(1), 1–19.

30 M. Y. Yang, S. V. Zybin, T. Das, B. V. Merinov, W. A. Goddard, E. K. Mok, H. J. Hah, H. E. Han, Y. C. Choi and S. H. Kim, *Adv. Energy Mater.*, 2023, **13**(3), 2202949.

31 D. Hou, M. Feng, J. Wei, Y. Wang, A. C. T. van Duin and K. H. Luo, *Chem. Eng. Sci.*, 2022, **252**, 117496.

32 D. J. Evans and B. L. Holian, *J. Chem. Phys.*, 1985, **83**(8), 4069–4074.

33 J. Lekner and J. R. Henderson, *Mol. Phys.*, 1977, **34**(2), 333–359.

34 R. He, P. Yi and T. Li, *Fuel*, 2023, **331**, 125729.

35 D. Zhou and P. Eames, *Sol. Energy Mater. Sol. Cells*, 2017, **167**, 157–161.

36 F. Kaufman and J. R. Kelso, *J. Chem. Phys.*, 1955, **23**(9), 1702–1707.

37 U. Olsher, R. M. Izatt, J. S. Bradshaw and N. K. Dalley, *Chem. Rev.*, 1991, **91**(2), 137–164.

38 L. Zhan, H. Chen, H. Zhou, Q. Feng, L. Gu, L. Yang and Z. Sun, *Appl. Therm. Eng.*, 2022, **213**, 118752.

39 J. Shinjo, J. Xia, L. C. Ganippa and A. Megaritis, *Phys. Fluids*, 2014, **26**(10), 103302.

40 H. Watanabe, Y. Matsushita, H. Aoki and T. Miura, *Combust. Flame*, 2010, **157**(5), 839–852.